

# Quantitative transmission electron microscopy analysis of multi-variant grains in present L1<sub>0</sub>-FePt based heat assisted magnetic recording media

Hoan Ho' , Jingxi Zhu' , Andreas Kulovits, David E. Laughlin, and Jian-Gang Zhu

Citation: *Journal of Applied Physics* **116**, 193510 (2014); doi: 10.1063/1.4902082

View online: <http://dx.doi.org/10.1063/1.4902082>

View Table of Contents: <http://aip.scitation.org/toc/jap/116/19>

Published by the *American Institute of Physics*

---

## Articles you may be interested in

[Growth of L1<sub>0</sub>-ordered crystal in FePt and FePd thin films on MgO\(001\) substrate](#)

*Journal of Applied Physics* **6**, 085302085302 (2016); 10.1063/1.4960554

---



Small Conferences. BIG Ideas.

Applied Physics  
Reviews

SAVE THE DATE!  
**3D Bioprinting: Physical and Chemical Processes**  
May 2–3, 2017 • Winston Salem, NC, USA

# Quantitative transmission electron microscopy analysis of multi-variant grains in present L1<sub>0</sub>-FePt based heat assisted magnetic recording media

Hoan Ho,<sup>1,2,a)</sup> Jingxi Zhu,<sup>3,4,b)</sup> Andreas Kulovits,<sup>2</sup> David E. Laughlin,<sup>1,2,3,5</sup> and Jian-Gang Zhu<sup>1,2,3,4,5</sup>

<sup>1</sup>Data Storage Systems Center, Carnegie Mellon University, Pittsburgh, Pennsylvania 15213, USA

<sup>2</sup>Department of Materials Science and Engineering, Carnegie Mellon University, Pittsburgh, Pennsylvania 15213, USA

<sup>3</sup>SYSU-CMU Joint Institute of Engineering, Sun Yat-Sen University, Guangzhou, China

<sup>4</sup>SYSU-CMU Shunde International Joint Research Institute, Guangdong, China

<sup>5</sup>Department of Electrical and Computer Engineering, Carnegie Mellon University, Pittsburgh, Pennsylvania 15213, USA

(Received 15 September 2014; accepted 7 November 2014; published online 20 November 2014)

We present a study on atomic ordering within individual grains in granular L1<sub>0</sub>-FePt thin films using transmission electron microscopy techniques. The film, used as a medium for heat assisted magnetic recording, consists of a single layer of FePt grains separated by non-magnetic grain boundaries and is grown on an MgO underlayer. Using convergent-beam techniques, diffraction patterns of individual grains are obtained for a large number of crystallites. The study found that although the majority of grains are ordered in the perpendicular direction, more than 15% of them are multi-variant, or of in-plane *c*-axis orientation, or disordered *fcc*. It was also found that these multi-variant and in-plane grains have always grown across MgO grain boundaries separating two or more MgO grains of the underlayer. The in-plane ordered portion within a multi-variant L1<sub>0</sub>-FePt grain always lacks atomic coherence with the MgO directly underneath it, whereas, the perpendicularly ordered portion is always coherent with the underlying MgO grain. Since the existence of multi-variant and in-plane ordered grains are severely detrimental to high density data storage capability, the understanding of their formation mechanism obtained here should make a significant impact on the future development of hard disk drive technology. © 2014 AIP Publishing LLC.

[<http://dx.doi.org/10.1063/1.4902082>]

## I. INTRODUCTION

Single variant L1<sub>0</sub>-FePt grains have very high magnetocrystalline anisotropy, enabling sufficient energy to be stored in each grain with several nanometer dimensions.<sup>1</sup> This particular property is one of the key reasons that granular L1<sub>0</sub>-FePt thin films are the leading candidate for heat assisted magnetic recording (HAMR), a technology geared for future hard disk drives (HDDs).<sup>2</sup> In current HDDs, data are stored on thin films of approximately 12 nm thickness, which consist of a single layer of magnetic grains about 7 nm in diameter with grains separated by a thin non-magnetic boundary phase. For the past 10 years, these grains have been cobalt-based alloys of an *hcp* crystal structure produced with their *c*-axes perpendicular to the film plane.<sup>3</sup> To continue the area density increase that we have been enjoying, the grain size of the media must be reduced. Consequently, the magnetocrystalline anisotropy strength of these grains must be increased to prevent thermally induced magnetic instability. However, the required anisotropy increase would also prevent the writing of data using the current recording scheme.

The high uniaxial magnetocrystalline anisotropy of a L1<sub>0</sub>-FePt arises from its atomically ordered superstructure in which the Fe and Pt atoms alternately occupy (002) crystal

planes causing the magnetic easy axis to be normal to the (002) plane.<sup>4</sup> The *fcc* to L1<sub>0</sub> phase transformation in FePt also results in an expansion in the *a*-axis and a compression in the *c*-axis, yielding a *c/a* ratio less than unity, *c/a* ≈ 0.96. See Fig. 1(a). In a (001) fiber textured film, there are two possible ordering directions, namely, out-of-plane (perpendicular) and in-plane as illustrated in Fig. 1(a), the former being the desired one. In addition, the associated decrease in crystal symmetry could also lead to structural multi-domains or variants within a single crystal grain. An ideal HAMR thin film recording media would consist of a layer of L1<sub>0</sub>-FePt grains which are all uniformly ordered with their easy axes in the direction perpendicular to film plane.<sup>5</sup> The existence of L1<sub>0</sub>-FePt grains with ordering directions in the film plane or of grains consisting of multi-variants would be detrimental to recording performance thereby limiting the area density capability of the media. Like the thin film disk media in current HDDs, industrial experimental HAMR media are also fabricated by a sputtering technique. FePt, together with a grain boundary phase material, usually carbon or an oxide, is sputtered at elevated temperature (usually above 550 °C), over a polycrystalline MgO underlayer with a strong (002) fiber texture.<sup>6</sup> The lattice constant of MgO, *a* = 4.21 Å, is 9.6% larger than that of FePt. It has been long believed that the lattice-coherence resulting in epitaxial growth of FePt over the MgO underlayer promotes the L1<sub>0</sub> ordering of the FePt grains in the direction perpendicular to the film during

<sup>a)</sup>Electronic mail: hoan.ho@wdc.com

<sup>b)</sup>Electronic mail: jingxiz@andrew.cmu.edu

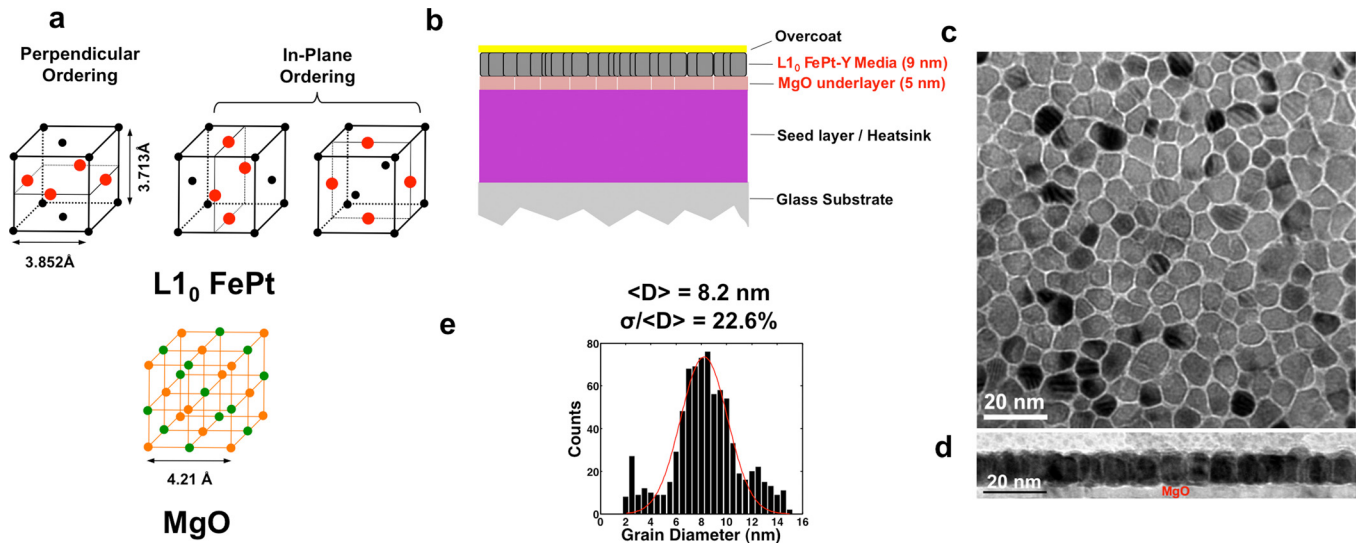


FIG. 1. Overview of the HAMR media under study. (a) Schematic of FePt unit cells in three structural domains and an MgO unit cell. (b) Schematic of the HAMR media layered stack (layer thicknesses are not drawn to scale). (c) and (d) Plane-view and cross-section TEM micrographs of the media. (e) Histogram of grain diameter showing a distribution with an average  $\langle D \rangle$  of 8.2 nm and a standard deviation  $\sigma/\langle D \rangle$  of 22.6%.

its deposition at elevated temperature owing to the in-plane bi-axial tension.<sup>7,8</sup>

It is critically important for all L1<sub>0</sub>-FePt grains in a film medium to be a single variant and ordered in the perpendicular direction. Variations in the L1<sub>0</sub> ordering at the grain level will cause severe recording performance degradation.<sup>9</sup> Quantitatively determining the amount of defective grains in L1<sub>0</sub>-FePt granular thin films using indirect techniques such as X-ray diffraction (XRD)<sup>10</sup> and magnetic measurements<sup>11,12</sup> is possible but challenging due to a requirement of robust peak deconvolution and model fitting, and a lack of standard samples for calibration. More importantly, these techniques provide limited information about the spatial location of ordering defects in the media thin films. Although the FePt microstructure has been studied for over a decade,<sup>12–14</sup> the origin of the unwanted ordering defects has not been elucidated, thus hindering the commercialization of the HAMR technology. This investigation was designed to examine fundamental aspects of the mechanism of the ordering defects and contribute to the solution of the microstructural issues related to recording performance. In this paper, we report on a transmission electron microscopy (TEM) based quantitative study of L1<sub>0</sub> atomic ordering at the grain level on a prototype HAMR media. In particular, the convergent electron beam diffraction (CEBD) technique is used to study the state of order (out-of-plane, in-plane, or mixed) of a large number of individual L1<sub>0</sub>-FePt grains.

## II. EXPERIMENT

The experimental HAMR disk was fabricated by sputter deposition on both sides of a 2.5-in.-diameter high temperature glass substrate. All the functional layers were deposited in a serial arrangement of multiple sputtering and heating stations. A schematic of the HAMR media studied here is shown in Fig. 1(b). It consists of a single layer of FePt grains with a non-magnetic grain boundary phase and the thickness

of the film is about 9 nm. The FePt layer was deposited on an MgO underlayer of a thickness of 5 nm at elevated temperature, while underneath the MgO layer is a film stack comprising an amorphous seedlayer and a heat sink layer on a glass disk substrate. From the plan-view micrograph in Fig. 1(c), small FePt grains are physically isolated by the grain boundary phase and have an average grain diameter of 8.2 nm with a 22.6% standard deviation. The cross-sectional view in Fig. 1(d) shows the FePt grains are columnar. The FePt grains have a chemical composition of  $56.0 \pm 1.5\%$  Fe and  $44.0 \pm 1.5\%$  Pt, determined by Energy Dispersive Spectroscopy (EDS) on the Scanning Transmission Electron Microscopy (STEM) mode. The lattice constants of FePt and MgO thin films measured from in-plane and perpendicular XRD scans are  $a_{\text{FePt}} = 3.84 \text{ \AA}$ ,  $c_{\text{FePt}} = 3.72 \text{ \AA}$ , and  $a_{\text{MgO}} = 4.18 \text{ \AA}$ . It has been shown that the slightly Fe rich off-stoichiometric composition offers the highest anisotropy which is beneficial for HAMR media applications.<sup>15</sup>

The analytical TEM study was performed utilizing a FEI Tecnai F20 with a field emission gun operated at an acceleration voltage of 200 kV. In the CEBD technique, the smallest spot size was used to achieve a convergent beam with approximately a 1 nm beam diameter such that the beam can be placed well within a single FePt grain in the medium sample. See Appendix A. The TEM thin foil specimens were prepared by mechanical thinning, dimple grinding, and followed by ion milling from the substrate side of the media. By controlling the Ar ion energy and milling grazing angles, wedge shaped areas were obtained along which different residual layers of interest can be used for analysis. See Appendix B. As shown in Fig. 2(a), region 1 is the thinnest area containing only the granular FePt films. In this area, the Convergent Beam Electron Diffraction (CBED) pattern arises from a single FePt grain. In region 2, the MgO underlayer has been retained, as indicated by additional diffraction patterns superimposed over that of the FePt as well as Moiré fringe patterns clearly seen in the bright field (BF) micrograph. In region 3 where the

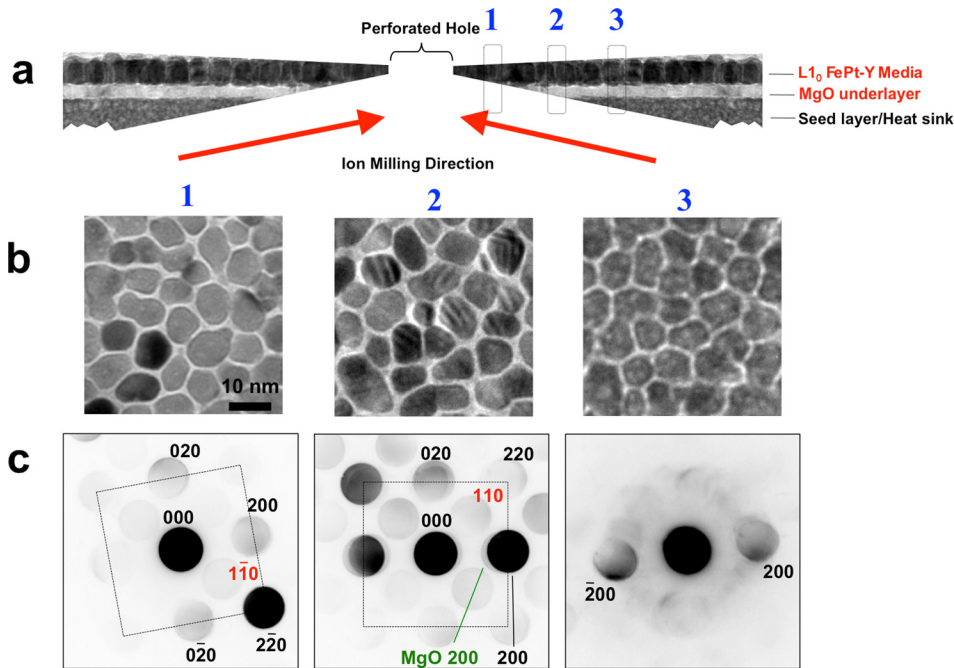


FIG. 2. Different thin foil regions for TEM analysis. (a) Schematic of the last Ar ion milling step to prepare the wedge-shaped plane view TEM specimen. (b) BF images of three regions denoted as 1, 2, and 3 which contain only the FePt media layer, FePt layer and MgO underlayer, and the FePt layer, MgO underlayer, and seedlayer; respectively. (c) Corresponding CBED patterns taken from an individual grain in regions 1, 2, and 3.

amorphous seed layer is included, the BF micrograph becomes somewhat fuzzy and the CBED pattern shows a diffraction ring of diffuse intensity owing to the remaining amorphous seedlayer. Region 1 was selected to analyze and quantify the defective FePt grains whereas region 2 was chosen to elucidate the possible mechanisms causing the FePt grains to grow improperly on the polycrystalline MgO underlayer.

### III. RESULTS AND DISCUSSION

#### A. Statistical results

The  $L1_0$  ordered state can be characterized by the observed diffraction patterns arising from the superlattice structure. Based on the calculations of the structure factors for  $L1_0$ ,  $hkl$  diffractions are superlattice if  $(h+k)$  is even and  $(h+l)$  is odd.<sup>16</sup> On the other hand, the  $hkl$  diffractions are fundamental when  $h$ ,  $k$ , and  $l$  are unmixed (all even or all odd). The  $(001)$  fiber texture of the thin film media makes it convenient to access  $\langle 100 \rangle$  zone axis patterns (ZAP) from a plane view TEM specimen. Furthermore, a  $\langle 100 \rangle$  ZAP provides unambiguous indication of the ordering states ( $L1_0/fcc$ ) and ordering orientation, i.e., in-plane or out-of-plane. Despite a fairly wide angular dispersion of the  $(001)$  texture (FWHM =  $8.0^\circ$ ), a large number of grains are in the zone axis without the need to use extensive tilting. We analyzed 94 randomly chosen individual grains one by one, from region 1 of the plane view specimen. It was found that the FePt grains exhibited four types of ordered states, namely, out-of-plane (OP) ordering, in-plane (IP) ordering, no ordering ( $fcc$ ), and multi-variant ordering, as displayed in Figs. 3(a)–3(h), respectively. A grain can be indexed as OP or IP ordering by the presence of  $110$  diffraction spots [Figs. 3(a) and 3(b)] or  $001$  diffraction spots [Figs. 3(c) and 3(d)], respectively. If the grain is  $fcc$  disordered, superlattice spots are missing from its CBED pattern as shown in Figs. 3(e) and 3(f). More

interestingly, we observed the presence of multi-variant grains having 2 or 3 structural domains which are ordered in orthogonal directions. Fig. 3(g) is an example of a bi-variant in which both  $110$  and  $001$  superlattice diffraction spots coexist from a single grain [Fig. 3(h)]. Out of 94 grains analyzed, the statistical fraction of each type summarized in Fig. 3(i) is 76% for OP ordering, 5% for IP ordering, 4% for multi-variant ordering, 11% for disordered ( $fcc$ ) and weakly ordered, and 4% for those grains orienting in high index zone axes.

#### B. Estimation of grain size of polycrystalline MgO underlayers

In order to understand the origin of the undesired grains (in-plane oriented, multi-variant, or  $fcc$  grains), the grain size of the polycrystalline MgO underlayers in the media was determined. A plane view micrograph usually includes several overlapped layers of the films.<sup>17</sup> The MgO layer is more “electron transparent” than the other layers in the media stack due to the small atomic scattering factors of Mg and O atoms. In addition, the microstructure of the MgO layer may change when subjected to exposure with air due to the hydrophilic nature of MgO.<sup>18</sup> Hence, direct measurement of the MgO grain size from BF imaging is very difficult. However, since most FePt grains epitaxially grow on MgO underlayers, the grain size of MgO underlayers could be indirectly measured by imaging the grains of FePt with the same in-plane orientation provided that the MgO grains are significantly larger than FePt grains. Orientation mapping of FePt grains was conducted to obtain an understanding of the grain size in the MgO underlayer. Diffraction patterns were recorded and their orientations determined by comparison with a template diffraction pattern bank in order to construct orientation maps with a point-to-point resolution of 1.0–1.3 nm as illustrated in Fig. 4(a) (Ref. 19). More details of the Orientation Imaging Microscopy (OIM) technique can be found in Appendix C. Figs. 4(b) and 4(c) show a virtual BF image and a corresponding in-plane

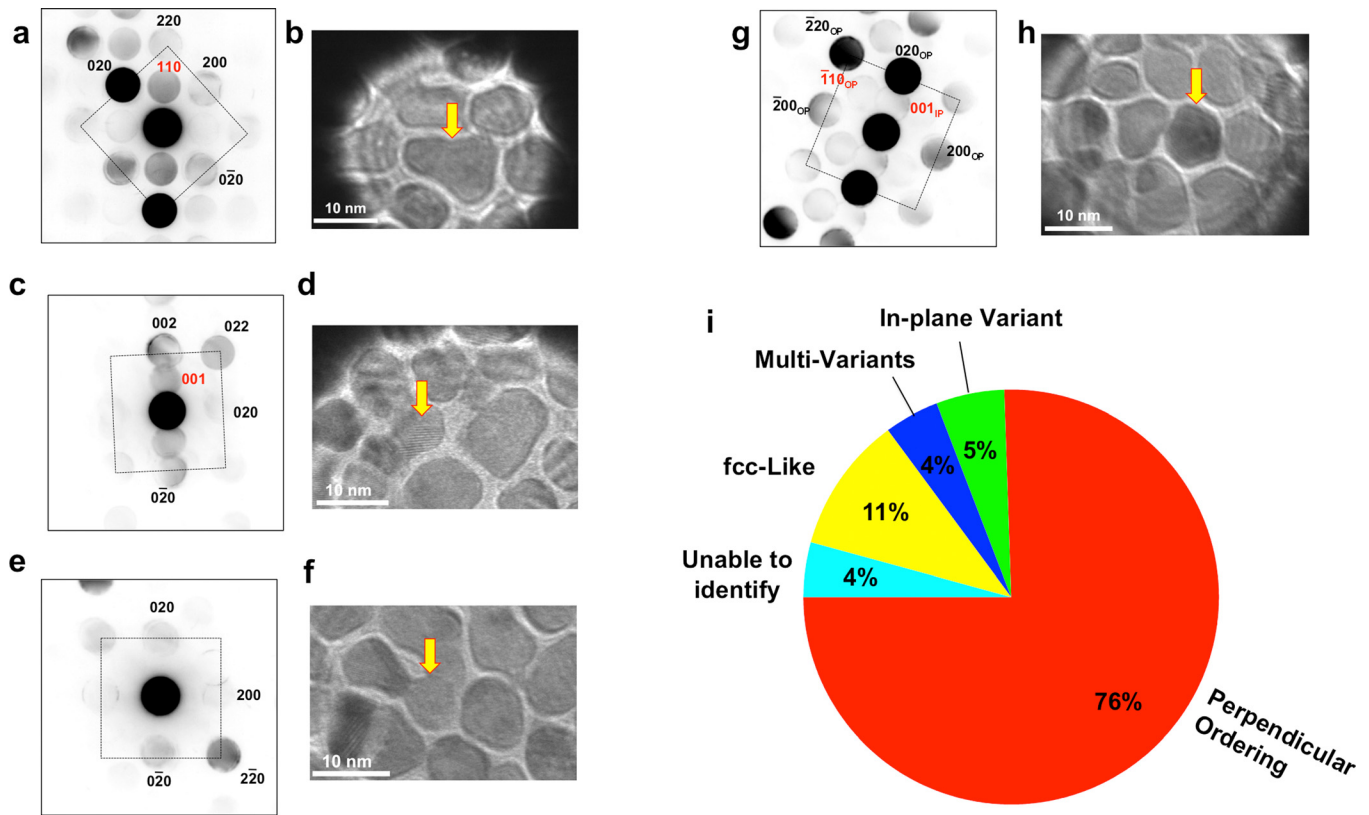


FIG. 3. Classification of  $L1_0$  ordered grains and their statistical contributions. (a) and (b) CBED pattern and its corresponding grain in BF presenting OP ordering. (c) and (d) CBED pattern and its corresponding grain in BF presenting IP ordering. (e) and (f) CBED pattern and its corresponding grain in BF presenting *fcc* (no ordering). (g) and (h) CBED pattern and its corresponding grain in BF presenting multi-variant ordering. (i) Pie chart showing fraction of each type.

orientation map, respectively. Clusters of FePt grains can be clearly seen, which share the same color. The cluster dimension is about 20 nm. This suggests that grain size of the polycrystalline MgO layer is at least 20 nm. This also means that a one-to-one grain registry between the MgO layer and the  $L1_0$ -FePt layer does not occur in the experimental HAMR media. Rather several FePt grains of the same orientation are formed on each MgO grain.

**C. Formation mechanism of multi-variant grains**

Next the role of the MgO grain boundaries on the ordering and orientation of the FePt grains was determined. Fig. 5

shows TEM micrographs and corresponding CBED patterns for two examples of OP grains with clearly visible Moiré striations. The diffraction patterns reveal perfect FePt(001)/MgO(002) || FePt[100]/MgO[100] epitaxial coherency. For all OP ordered grains, the above coherent orientation relationship has been observed. It is noted that because the magnitude of the  $g_{hkl}$  vectors in reciprocal space are inversely related to the  $hkl$  planar spacing in real space, MgO spots are close to the FePt fundamental spots in the CBED pattern. One can also confirm the coherency of FePt/MgO from the periodicity and orientation direction of the Moiré fringes. The Moiré patterns in BF images arise from interference

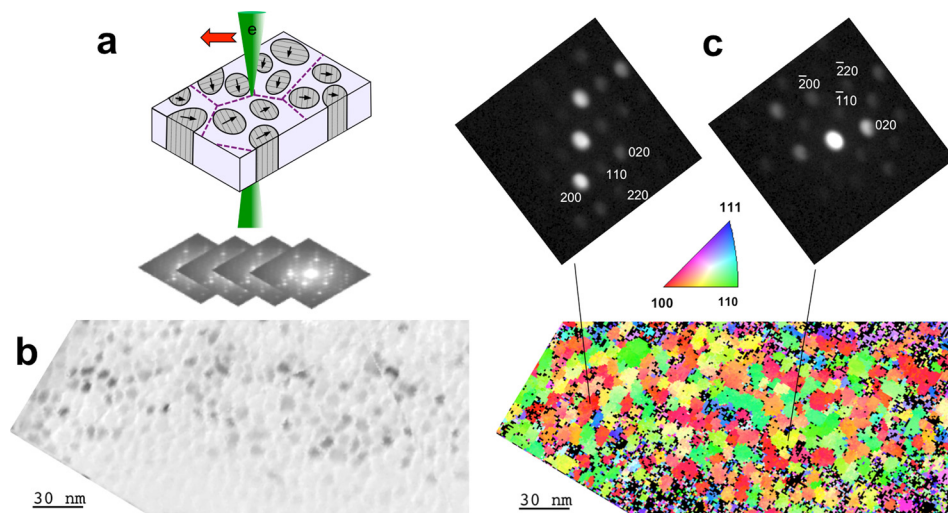


FIG. 4. Estimates of MgO grain size. (a) Schematic illustration of the Orientation Imaging Microscopy (OIM) technique used to determine FePt cluster size which in turn provides estimates of MgO underlayer grain size.<sup>19</sup> (b) Virtual BF image generated from the orientation mapping scan. (c) Orientation mapping of FePt grains shows grain clusters of about 20 nm in dimension.

between FePt and MgO diffraction spots in excited rows described by reciprocal vectors  $g_{FePt}$  and  $g_{MgO}$  and are perpendicular to  $\Delta g$  vector between  $g_{FePt}$  and  $g_{MgO}$ .<sup>20,21</sup> The periodicity  $\lambda_M$  is therefore given by

$$\lambda_M = \frac{1}{|g_{FePt} - g_{MgO}|} = \frac{d_{FePt}d_{MgO}}{\sqrt{d_{FePt}^2 + d_{MgO}^2 - 2d_{FePt}d_{MgO}\cos\alpha}}, \quad (1)$$

where  $d_{FePt}$ ,  $d_{MgO}$ , and  $\alpha$  are planar spacings and a relative angle of rotation between FePt(001) and MgO(002) from a cube-on-cube relation, respectively. When the epitaxial coherency is perfect,  $\alpha$  is equal to  $0^\circ$ . The directions of the Moiré patterns in Figs. 5(a) and 5(c) are consistent with the well-aligned excited rows along  $[2\bar{2}0]$  and  $[200]$  in Figs. 5(b) and 5(d), respectively. The measured Moiré pattern spacings are  $\sim 1.6$  nm and  $\sim 2.2$  nm, which are very close to the values of 1.59 nm and 2.36 nm evaluated by Eq. (1) using (220) and (200) inter-planar spacings (calculated from  $a_{FePt}$  and  $a_{MgO}$ ) when the tilt angle  $\alpha$  is  $0^\circ$ .

Multi-variant  $L1_0$ -FePt grains have been observed and studied intensively in bulk<sup>22,23</sup> and chemically synthesized nanoparticles.<sup>24,25</sup> Their existence is explained by the fact that the systems try to reduce the strain energy between nucleus and matrix associated with the distortion of an  $L1_0$  phase nucleating from an *fcc* matrix. The boundaries between these domains are usually planes of the type  $\{101\}$ . The nucleation and growth ordering transformation mostly occurs in post annealing or *ex situ* heating which is how bulk and synthesized nanoparticles are processed. The HAMR media thin films are, however, deposited under *in situ* heating conditions. The transition is continuous in which the

films start with small chemical order and progressively increase with time. Therefore, the ordered nuclei are most likely to be spontaneously formed upon impinging onto the heated substrate. The lattice constant of MgO is about 9.6% greater than that of FePt. Atomic coherence between the two would cause in-plane biaxial tension and perpendicular compression in FePt, which favors out-of-plane ordering since the *c/a* ratio is less than unity. Such a mechanism drives the formation of OP grains when FePt coherently grows on the MgO underlayer as shown above.

Fig. 6(a) shows a BF micrograph of the FePt grains with the MgO underlayer present. The Moiré fringe pattern of the grain highlighted in the middle suggests that the left region (indicated by the red L) and right region (indicated by the red R) of the FePt grain are over two different underlying MgO grains schematically illustrated in Fig. 6(d). Figs. 6(b) and 6(c) show the CBED patterns for the region L and region R, respectively. The CBED patterns show that while the FePt grain is a single fundamental lattice over the two regions, the region R is ordered out-of-plane and region L is ordered in-plane, both of  $L1_0$  superlattice. The out-of-plane ordering region shows atomic coherence between the FePt and MgO underlayer as the superimposed diffraction patterns from the MgO underlayer shows. However in the case of the in-plane ordered region, the underlayer MgO lattice is  $12.2^\circ$  tilted from that of the FePt. The spacing and orientation of the Moiré fringes on the portion L and R are in very good agreement with their corresponding CBED patterns observed. Figs. 6(e)–6(h) constitute a second example of a bi-variant FePt atop two neighboring MgO grains. Fig. 6(e) is a BF micrograph of the FePt grain that also displays two regions with different Moiré fringe

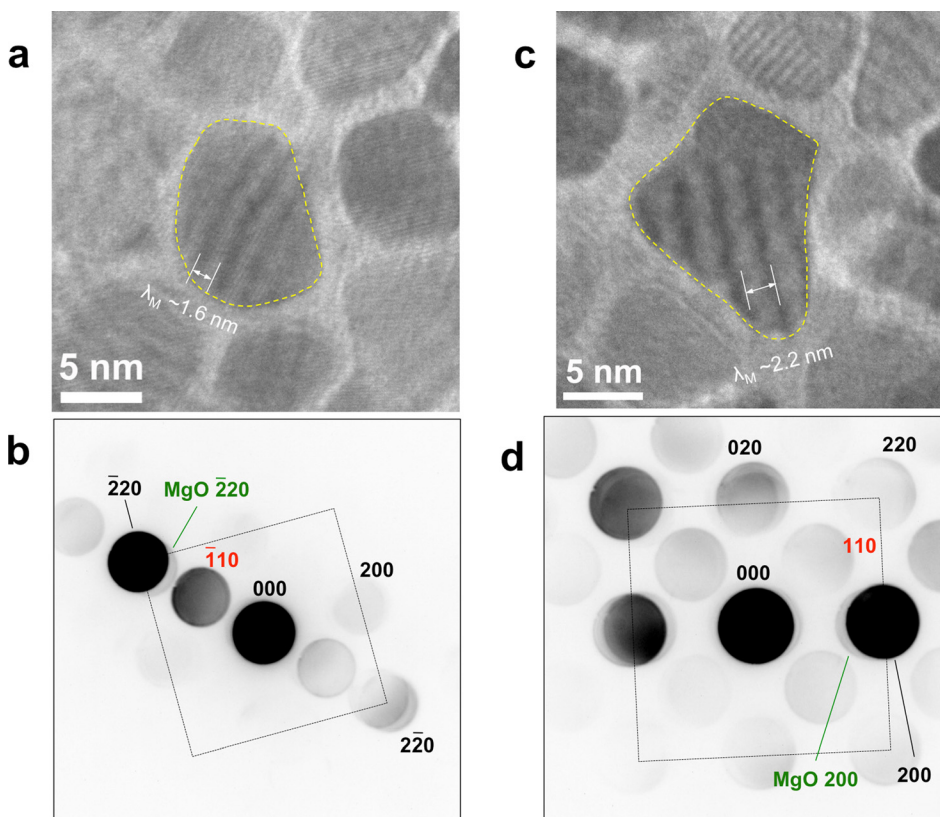


FIG. 5. Coherent epitaxial growth of FePt on MgO underlayers assists OP ordering. (a) BF image showing Moiré fringes due to interference between FePt(-220) and MgO(-220) planes. (b) Corresponding CBED pattern of the grain in (a). (c) BF image showing Moiré fringes due to interference between FePt(200) and MgO(200) planes. (d) Corresponding CBED pattern of the grain in (c).

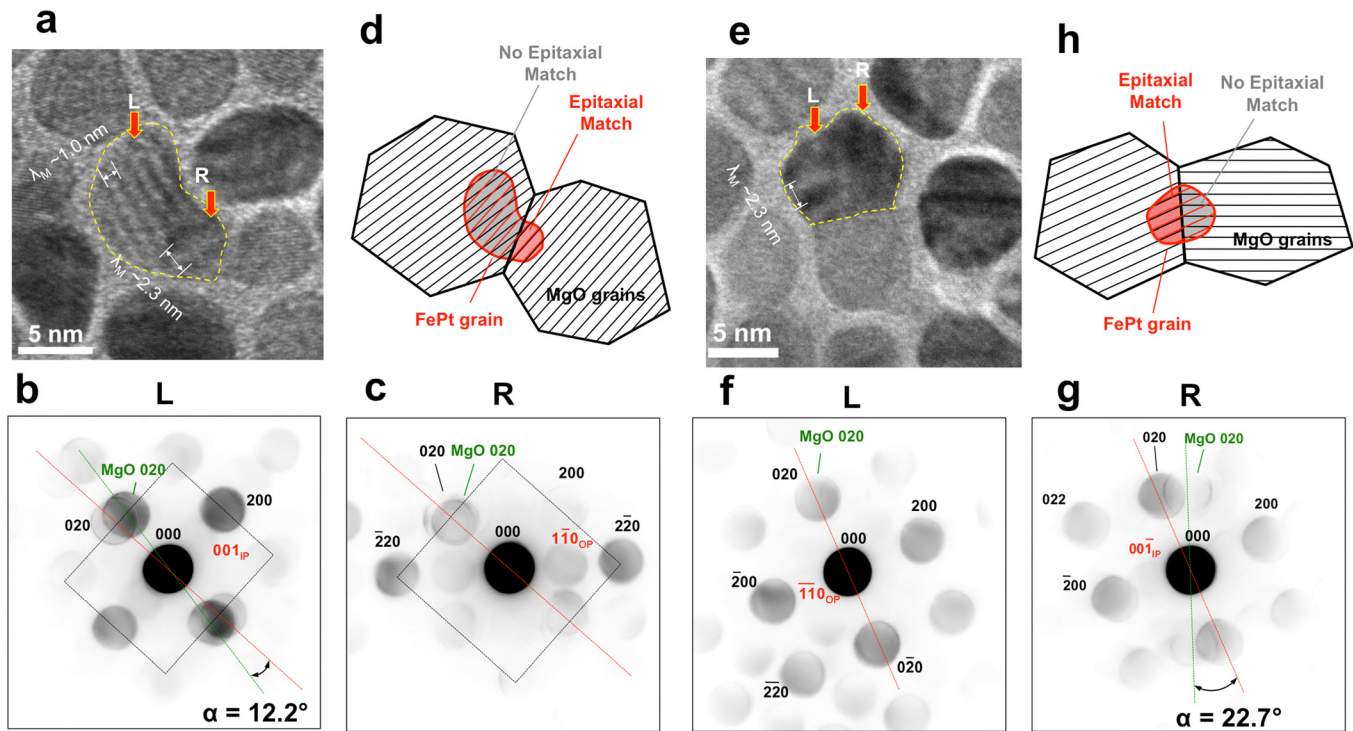


FIG. 6. Extended growth of FePt over neighboring MgO grain results in bi-variant grains. (a) BF image of a bi-variant grain. (b) and (c) CBED patterns of the portion L and R, respectively. (d) Schematic illustration of the growth of the FePt nucleus from the right MgO grain over to the left MgO grain. (e) BF image of a bi-variant grain. (f) and (g) CBED patterns of the portion L and R, respectively. (h) Schematic illustration of the growth of the FePt nucleus from the left MgO grain over to the right MgO grain.

patterns. The corresponding CBED patterns [Figs. 6(f) and 6(g)] reveal that the left region of the FePt  $L1_0$  grain, region L, is ordered out-of-plane with lattice coherence with the MgO grain underneath whereas the right region, region R, is in-plane ordered and the lattice of the MgO grain underneath this region is oriented away from that of the FePt grain with an angle of  $22.7^\circ$ . This is illustrated in Fig. 6(h). Multi-variant grains (all of them bi-variant) investigated using this methodology all show the same phenomenon.

The above observations over the multi-variant FePt grains suggest the following mechanism for the formation of the multi-variants. When a FePt grain nucleates, it always starts with a coherent epitaxial orientation on top of the MgO grain and the region with the lattice coherence is ordered in the out-of-plane direction due to the in-plane bi-axial tensile strain which arises from its coherency with the MgO lattice. However, if the subsequent lateral growth of the FePt grain crosses over an MgO grain boundary to a different MgO grain underneath, the coherence in the region over the new MgO grain is lost. Consequently, the region of the FePt grain extended over the new MgO grain will not have the in-plane bi-axial tensile strain. Without the preference for yielding the ordering in the out-of-plane direction, the region would have approximately a 2/3 probability to order in-plane.

The understanding of formation mechanism obtained here provides insights into development of new methods to eliminate or at least minimize the defective grain concentration. Growing MgO layers with significantly larger grain size is one possible approach since MgO films with larger grains will have less grain boundary density, and hence will

potentially decrease amounts of multi-variants and/or in-plane variants. In fact, it has been experimentally observed when single crystal MgO (001) substrates are used for epitaxial growth of FePt-C granular thin films, one obtains significantly reduced in-plane grains as opposed to polycrystalline MgO underlayers.<sup>26</sup> An alternative approach, which is much more challenging, is to achieve an one-to-one epitaxial growth mode between FePt grains and underlayer's grains. In order to pursue this direction, one needs to design and develop a new underlayer or underlayer system, which possesses a comparable average grain size of that of FePt thin films and is capable of enforcing grain registry.

#### IV. CONCLUSION

$L1_0$  ordering in the FePt based granular magnetic thin film as recording media for HAMR applications has been studied at the grain level using the convergent beam electron diffraction technique. Although a majority of the  $L1_0$ -FePt grains are ordered with  $c$ -axis perpendicular to the film plane that exhibit lattice coherence with the MgO underlayer, a small, but significant, percentage of the  $L1_0$ -FePt grains are found to be multi-variant. The study found that these multi-variant  $L1_0$ -FePt grains are formed by first nucleating on one MgO grain with lattice coherence followed by grain growth extending over to a neighboring MgO grain where lattice coherence are no longer maintained. This finding suggests a grain with an in-plane component of ordering will probably also contain a perpendicular ordering component. Thus, the 5% in-plane ordered grains characterized in the pie chart shown in Fig. 3(i) could very

well be multi-variant grains considering the fact that the probe size is significantly smaller than the FePt grain size.

The MgO grain size is estimated by studying the in-plane orientation of FePt grains using TEM based diffraction mapping. It was found that MgO grain size is significantly larger than that of the FePt grains and multiple FePt grains nucleate on a single MgO grain. This fact facilitates the over-growth of some FePt grains across MgO grain boundaries, resulting in possible multi-variant  $L1_0$  ordering. One-to-one grain matching between the FePt and MgO grains with complete lattice coherence would potentially eliminate this cause, preventing the formation of multi-variant grains.

## ACKNOWLEDGMENTS

This research was supported in part by the Data Storage Systems Center at Carnegie Mellon University and its industrial sponsors. The authors would also like to thank many helpful discussions with engineers from Seagate Technology, Western Digital, HGST-a WD company, and Showa Denko.

## APPENDIX A: CBED TECHNIQUE

All electron microscopy analyses were conducted on a FEI Tecnai F20 Super-Twin field emission TEM/STEM operating at a high tension of 200 kV. The CBED experiment was carried out using convergent beam probe at the smallest spot size 11, which was measured to be about 1 nm from the full width half maximum of the Gaussian spot. The condenser aperture was set at 50  $\mu\text{m}$ , which gives a convergence angle of  $<2$  mrad for the beam. The CBED patterns were recorded with an acquisition time of 5 s using a Gatan Orius 2672  $\times$  2672 CCD camera.

## APPENDIX B: TEM SPECIMEN PREPARATION

Plan-view TEM specimen preparation follows a conventional method. The medium was first cut into  $5 \times 5 \text{ mm}^2$  pieces. Each sample was initially mechanically ground and polished from the substrate back-side using silicon carbide abrasive papers down to less than 60  $\mu\text{m}$  in thickness. The samples were further back-thinned using a Gatan-656 dimple grinder to a thickness of less than 10  $\mu\text{m}$  at the center. Then, after being glued into standard 3 mm diameter copper grids, the samples were ion milled with Ar ion at 3.5 keV and an incident angle of  $8.5^\circ$  using a Gatan precision ion polishing system II (PIPS<sup>TM</sup> II). Once holes were perforated, the beam energy and the beam angle were reduced to 0.5 keV and  $6^\circ$ , respectively, for 4 min to clean the damaged regions. Areas of the thin layers of interest near the holes are electron transparent and used for TEM analytical characterization.

## APPENDIX C: ORIENTATION IMAGING MICROSCOPY (OIM) TECHNIQUE

For the estimation of the grain size of the MgO, we used a novel TEM based automated OIM technique. OIM in the TEM (ASTAR<sup>TM</sup> system from NanoMEGAS, Brussels,

Belgium) allows quantitative measurements of grain orientations, grain boundary characters, local texture, and phase identification with nm spatial resolution.<sup>19</sup> This system combines an about the optical axis of the TEM precessed parallel incident electron beam to acquire easy to index precession illumination diffraction pattern (PI-DP) with beam scanning to acquire orientation and phase maps. As dynamic beam interaction effects are significantly reduced in PI-DP, the observed diffraction maxima can be treated kinematically, which allows the easy and robust PI-DP indexing, and thereby quantitative phase and orientation determination.<sup>19,27</sup> Like SEM based EBSD techniques, orientation and phase maps are constructed through indexing of the acquired Pi-DP for every scanned position  $x,y$  (Ref. 19). In difference to the SEM based EBSD methods where the spatial resolution is limited by the size of the electron probe-sample interaction volume, resolution of the TEM based OIM approach is only limited by the probe size of the TEM.

<sup>1</sup>D. Weller, A. Moser, L. Folks, M. E. Best, L. Wen, M. F. Toney, M. Schwickert, J. U. Thiele, and M. F. Doerner, *IEEE Trans. Magn.* **36**(1), 10–15 (2000).

<sup>2</sup>M. H. Kryder, E. C. Gage, T. W. McDaniel, W. A. Challener, R. E. Rottmayer, J. Ganping, H. Yiao-Tee, and M. F. Erden, *Proc. IEEE* **96**(11), 1810–1835 (2008).

<sup>3</sup>H. J. Richter, *J. Phys. D: Appl. Phys.* **40**, R149 (2007).

<sup>4</sup>D. E. Laughlin, K. Srinivasan, M. Tanase, and L. Wang, *Scr. Mater.* **53**(4), 383–388 (2005).

<sup>5</sup>J. G. Zhu, Y. G. Peng, and D. E. Laughlin, *IEEE Trans. Magn.* **41**(2), 543–548 (2005).

<sup>6</sup>D. Weller, O. Mosendz, G. Parker, S. Pisana, and T. S. Santos, *Phys. Status Solidi A* **210**(7), 1245–1260 (2013).

<sup>7</sup>Y.-N. Hsu, S. Jeong, D. E. Laughlin, and D. N. Lambeth, *J. Magn. Magn. Mater.* **260**(1-2), 282–294 (2003).

<sup>8</sup>P. Rasmussen, X. Rui, and J. E. Shield, *Appl. Phys. Lett.* **86**(19), 191915 (2005).

<sup>9</sup>D. Weller, G. Parker, O. Mosendz, E. Champion, B. Stipe, X. Wang, T. Klemmer, G. Ju, and A. Ajan, *IEEE Trans. Magn.* **50**(1), 1–8 (2014).

<sup>10</sup>H. Ho, D. E. Laughlin, and J. G. Zhu, *IEEE Trans. Magn.* **48**(11), 2749–2752 (2012).

<sup>11</sup>S. Pisana, O. Mosendz, G. J. Parker, J. W. Reiner, T. S. Santos, A. T. McCallum, H. J. Richter, and D. Weller, *J. Appl. Phys.* **113**(4), 043910 (2013).

<sup>12</sup>S. Wicht, V. Neu, L. Schultz, D. Weller, O. Mosendz, G. Parker, S. Pisana, and B. Rellinghaus, *J. Appl. Phys.* **114**(6), 063906 (2013).

<sup>13</sup>T. Miyazaki, O. Kitakami, S. Okamoto, Y. Shimada, Z. Akase, Y. Murakami, D. Shindo, Y. K. Takahashi, and K. Hono, *Phys. Rev. B* **72**, 144419 (2005).

<sup>14</sup>Y. Peng, T. Ohkubo, and D. E. Laughlin, *Scr. Mater.* **48**(7), 937–942 (2003).

<sup>15</sup>K. Barmak, J. Kim, L. H. Lewis, K. R. Coffey, M. F. Toney, A. J. Kellock, and J.-U. Thiele, *J. Appl. Phys.* **98**(3), 033904 (2005).

<sup>16</sup>B. E. Warren, *X-ray Diffraction* (Addison-Wesley Publishing Company, Reading, Massachusetts, 1969).

<sup>17</sup>D. E. Laughlin, N. T. Nuhfer, S. Park, H. Yuan, and J.-G. Zhu, *J. Appl. Phys.* **105**(7), 07B739 (2009).

<sup>18</sup>M. Odellius, *Phys. Rev. Lett.* **82**(19), 3919–3922 (1999).

<sup>19</sup>P. Moecq, S. Rouvimov, E. F. Rauch, M. Véron, H. Kirmse, I. Häusler, W. Neumann, D. Bultreys, Y. Maniette, and S. Nicolopoulos, *Cryst. Res. Technol.* **46**(6), 589–606 (2011).

<sup>20</sup>D. B. Williams and C. B. Carter, *Transmission Electron Microscopy: A Textbook for Materials Science*, 2nd ed. (Springer Science+Business Media, LLC, New York, 2009).

<sup>21</sup>F. Hossein-Babaei, R. Sinclair, K. Srinivasan, and G. A. Bertero, *Nano Lett.* **11**(9), 3751–3754 (2011).

<sup>22</sup>T. Klemmer, D. Hoydick, H. Okumura, B. Zhang, and W. A. Soffa, *Scr. Metall. Mater.* **33**(10–11), 1793–1805 (1995).

<sup>23</sup>L.-Q. Chen, Y. Wang, and A. G. Khachatryan, *Philos. Mag. Lett.* **65**(1), 15–23 (1992).

<sup>24</sup>F. Tournus, K. Sato, T. Epicier, T. J. Konno, and V. Dupuis, *Phys. Rev. Lett.* **110**, 055501 (2013).

<sup>25</sup>B. Bian, D. E. Laughlin, K. Sato, and Y. Hirotsu, *J. Appl. Phys.* **87**(9), 6962–6964 (2000).

<sup>26</sup>B. S. D. C. S. Varaprasad, T. Shiroyama, K. Takahashi, and K. Hono, personal communication (Sep 2013).

<sup>27</sup>A. K. Kulovits, G. Facco, and J. M. K. Wiezorek, *Mater. Charact.* **63**, 17–26 (2012).